Journal of Materials Chemistry A

COMMUNICATION

Check for updates

Cite this: J. Mater. Chem. A, 2017, 5, 13357

Received 11th May 2017
Accepted 12th June 2017

DOI: 10.1039/c7ta04101b

rsc.li/materials-a

Ultra-stretchable ionic nanocomposites: from dynamic bonding to multi-responsive behavior†

J. Odent, [a] J.-M. Raquez,[b] Ph. Dubois*[bc] and E. P. Giannelis*[a]

Although multi-responsive materials have the potential to revolutionize a wide spectrum of technologies, the design of systems that combine a range of responses to a variety of different external changes without the associated property trade-offs has remained elusive. We herein demonstrate a new family of multi-responsive nanocomposites that leverage the dynamic and reversible nature of electrostatic interactions present in ionic systems with the reinforcement ability of nanoparticles in nanocomposites. This new design leads to a unique property profile that combines simultaneous improvements in stiffness, toughness and extensibility. In addition to their exceptional stretchability, the new, ionic nanocomposites exhibit unique strain-dependent behavior (*i.e.* the deformation increases with increasing strain rates) and return to the normal state after deformation including shape-memory and scratch recovery.

Introduction

Over the last several years, dynamic polymer systems, where specific bonds or interactions can selectively undergo reversible breaking and restoration under certain conditions have attracted widespread attention.[1–3] This design offers the possibility to endow materials with multi-responsive properties from stimuli-responsiveness to shape-memory and self-healing.[4–9] A variety of dynamic interactions, such as multiple hydrogen bonding,[10–12] hydrophobic interactions,[13–15] π–π stacking,[16,17] metal–ligand coordination[18,19] and ionic bonding,[20–23] have been used to design such systems. An alternative strategy involves covalent bond exchange in a polymer network (such as by metal-catalyzed transesterification) allowing rearrangements in response to an external force.[24–26] Ionomers represent another class of dynamic polymers.[27–29] For instance, Surlyn®, a commercial poly(ethylene-*co*-methacrylic acid)-based thermoplastic ionomer manufactured by DuPont, offers both one-way multishape-memory effects and tunable two-way reversible actuation.[30] Multishape-memory effects and tunable dual-shape memory behavior were demonstrated for Zn^{2+} ion-exchanged Surlyn® by leveraging the broad melting temperature range of the ionomer.[31] This behavior was attributed to the interplay of the permanent cross-linked network formed by the ionic clusters and the temporary network provided by the polyethylene crystalline domains.[30,31] Such ionic clusters are also known to play a vital role in the self-healing process of ionomers because of their reversibility.[32] Meanwhile, the growing interest in nanoparticles led to the design of several systems based on surface-functionalized nanoparticles.[33] A subset of such nanoparticles, referred to as nanoscale ionic materials (NIMs), consists of a soft polymeric canopy bound to a well-defined nanoparticle core by ionic interactions.[34–37] Thanks to the ionic interactions present, the perennial dispersion challenges associated with conventional nanocomposites are minimized while the dynamic nature of the ionic bonds provides opportunities for adaptive/multi-responsive properties.[37] Jespersen *et al.*[38] successfully characterized the molecular-level dynamics in NIMs and demonstrated that the polymeric canopy undergoes rapid exchange. Exploiting the unique properties of the inherent ionic interactions in the NIMs can lead ultimately to exquisite control of both the structure and dynamics using a simple, yet versatile, material platform suitable for a wide range of applications.[33–38]

Building on this ionic motif, we previously showed that conventional, non-responsive polylactide (PLA) can be endowed with shape-memory behavior by blending commercial PLA with imidazolium-terminated glassy PLA and rubbery poly[ε-caprolactone-*co*-D,L-lactide] oligomers and adding surface-modified silica nanoparticles.[39] Although this contribution

[a]*Department of Materials Science and Engineering, Cornell University, Ithaca, NY 14853, USA. E-mail: epg2@cornell.edu*

[b]*Laboratory of Polymeric and Composite Materials (LPCM), Center of Innovation and Research in Materials and Polymers (CIRMAP), University of Mons (UMONS), 23 Place du Parc, 7000 Mons, Belgium. E-mail: philippe.dubois@umons.ac.be*

[c]*National Composite Center-Luxembourg, Luxembourg Institute of Science and Technology, 5 rue Bommel, 4940 Hautcharage, Luxembourg*

† Electronic supplementary information (ESI) available. See DOI: 10.1039/c7ta04101b

demonstrated some of the potential advantages of introducing electrostatic interactions in the hybrids, the system remained complex and challenging to implement. In an effort to extend the design to a broader class of polymer systems we report here a new class of adaptable/multi-responsive ionic nanocomposite materials. The materials are based on the imidazolium-functionalized polyurethane canopy (im-PU) and surface-modified sulfonated silica nanoparticles (nanosilica-SO_3H). The hybrid nature allows for their properties to be readily engineered by selectively varying the system components and the reversible nature of the ionic bonds introduces unprecedented structural and dynamic behavior in the nanocomposites, which were unrealized in our earlier work. Specifically, the nanocomposites are stiff, tough and highly deformable with remarkable recovery of deformation. The latter characteristic allows the nanocomposites to recover after extensive deformation and self-heal. The combination of enhanced mechanical performance with reversible plasticity/shape-memory and self-healing properties provides unique opportunities for current and future applications and makes these nanocomposites potential candidates for use in several engineering and biomedical fields.

Experimental

Materials

Hexamethylene diisocyanate (HMDI, >98%, Aldrich) and dibutyltin dilaurate (DBTDL, 95%, Sigma) were stored in a glovebox. Polyethylene glycol (PEG, 2000 g mol^{-1}, Sigma), poly(ethylene glycol-*ran*-polypropylene glycol) (PEG-*ran*-PPG, 2500 g mol^{-1}, Sigma), 2,2-bis(bromomethyl)propane-1,3-diol (BBPDO, 98%, Sigma), Ludox HS 30 colloidal silica (mean diameter 18 nm, Aldrich), 3-(trihydroxysilyl)-1-propane sulfonic acid (SIT, 40 wt%, Gelest), sodium hydroxide solution (1 M, Aldrich), 1-methyl-imidazole (99%, Aldrich), anhydrous tetrahydrofuran (THF, >99.8%, packaged under argon, Alfa Aesar), *N*,*N*-dimethylformamide (DMF, >99.7%, packaged under argon, Alfa Aesar), dialysis tubing (Spectra/Por RC Biotech Membrane, 15k MWCO, 16 mm flat width) and ion exchange resin (Dowex, HCR-W2 ion exchange resin) were purchased as indicated and used without further purification.

Ionic nanocomposite preparation

Imidazolium-functionalized polyurethanes were synthesized by the reaction of 1.2 eq. of hexamethylene diisocyanate with 0.9 eq. of polyethylene glycol-based (PEG or PEG-*ran*-PPG) oligomer, 0.1 eq. of imidazolium-based diol and catalytic amounts of dibutyltin dilaurate in DMF at 60 °C for 6 h under nitrogen. Meanwhile, sulfonate functionalized silica nanoparticles were prepared following a previously reported method.[34] Dissolving the as-synthesized polyurethanes in deionized water followed by the addition of the sulfonated silica suspension and freeze-drying then allow the formation of the nanocomposite. Thin films of the resulting nanocomposite were prepared by compression-molding. Further details on the methods are available in the ESI with the synthesis shown schematically in Fig. S1.†

Characterization techniques

Rheological measurements were performed using an Anton Paar Physica Modular Compact Rheometer 501 (MCR-501). A cone and plate system was used with a 25 mm diameter. All measurements were performed at 60 °C with a strain of 1% to ensure that the deformations are in the linear viscoelastic regime. Tensile tests were performed according to ASTM D638 using a Zwick universal tensile testing machine (Ulm, Germany). Transmission electron microscopy (TEM) was carried out using an FEI Tecnai T12 Spirit Twin TEM/STEM microscope operated at 120 kV. Samples were cryo-microtomed at −100 °C with a Leica UCT microtome. Dynamic mechanical thermal analyses (DMTA) were performed under ambient atmosphere using a strain-controlled DMTA Q800 apparatus from TA Instruments in a film tension mode. Proton nuclear magnetic resonance (^{1}H NMR) spectra were recorded in DMSO using a Bruker AMX-400 apparatus at 400 MHz. Size-exclusion chromatography (SEC) was performed in THF at 35 °C using an Agilent liquid chromatograph equipped with an isocratic HPLC pump G1310A (flow rate: 1 mL min^{-1}), autosampler G1329A (loop volume: 100 μL, solution concentration: 1 mg mL^{-1}), and three columns: a guard column PLgel 10 μm and two columns PLgel mixed-B 5 μm. Molecular weights and molecular weight distribution were calculated by reference to a relative calibration curve made of polystyrene standards. Differential scanning calorimetry (DSC) was performed using a DSC Q2000 (TA Instruments) at heating and cooling rates of 10 °C min^{-1} under nitrogen flow; to avoid any thermal history effects the 2nd scan was used. Thermal gravimetric analysis (TGA) was performed using a TGA Q500 from TA Instruments at a heating rate of 20 °C min^{-1} under nitrogen flow. Dynamic Light Scattering (DLS) was carried out on samples in water (concentration of *ca.* 1 wt%) at 25 °C using a Malvern Zetasizer.

Shape recovery

Samples for shape recovery testing were cut from compression-molded thin films into rectangular shape-memory specimens of *ca.* 30 × 5 × 0.2 mm. Dynamic mechanical thermal analyses (DMTA) on these specimens were performed under ambient atmosphere using a strain-controlled DMTA Q800 apparatus from TA Instruments in a film tension mode. The shape recovery was characterized using the following four-step sequence: (1) deformation: the sample is first stretched at room-temperature (*i.e.* 20 °C) to a strain of 200% at a rate of 20% min^{-1}; (2) fixing in place: the sample is held at 200% strain for 10 min to allow stress relaxation; (3) unloading: the stress/force is released within 3 min, after which a large percentage of plastic deformation remained; and (4) heating and recovery: the sample is heated to 50 °C at a rate of 2 °C min^{-1} and then ramped back to 20 °C to complete the cycle. The ability of the materials to recover from substantial deformation is characterized by the sum of the elastic springback C_{elas} (*i.e.* recovery at room-temperature) and plastic springback C_{plas} (*i.e.* recovery upon heating), which provide the total deformation recovery, C_{tot}. In addition, shape fixity R_f and shape recovery R_r ratios are two key parameters used to describe the shape-memory

 This journal is © The Royal Society of Chemistry 2017

behavior of the materials.[40] They were calculated using the following equations:

$$C_{elas} = \frac{\varepsilon_s}{\varepsilon_{pr}},\ C_{plas} = \frac{\varepsilon_{rec}}{\varepsilon_{pr}},\ C_{tot} = C_{elas} + C_{plas}$$

$$R_f = \frac{\varepsilon_{res}}{\varepsilon_{pr}},\ R_r = \frac{\varepsilon_{rec}}{\varepsilon_{res}}$$

where ε_{pr} is the total programming strain obtained before the constant strain was released, ε_s and ε_{res} are respectively the elastic springback strain and the residual visco-plasto-damage strain directly after unloading at room temperature, and ε_{rec} is the recoverable strain obtained directly after heating the sample. The actuation program was repeated three times and good reproducibility was observed.

Scratch recovery

Surface scratches with a residual depth of *ca.* 500 μm and a width of *ca.* 160 μm were made at 25 °C through the samples. Qualitative scratch recovery after heating at 50 °C was evaluated using an optical microscope (OLYMPUS BX51) over time.

Results and discussion

Design of ionic nanocomposites

The new nanocomposites leverage the electrostatic interactions of imidazolium-functionalized polyurethanes (im-PUs, *ca.* 0.1 mmol g^{-1}) and surface-modified sulfonate silica nanoparticles (nanosilica-SO_3H, *ca.* 1 mmol g^{-1}) (Fig. 1). The proximity of the cationic imidazolium rings to the anionic sulfonate groups is the result of maximizing Coulomb interactions.[41] Building on the double-network principle,[42–45] the new nanocomposites are made of a 50/50 wt% ratio of a semi-crystalline im-PEG ionomer with an amorphous im-PEG-*ran*-PPG ionomer (noted as im-PU) ionically bonded to the nanosilica-SO_3H. As will be shown below, this motif allows the nanocomposites to combine the reinforcing effects of silica nanoparticles with the reversibility endowed to ionic systems. The theoretical charge balance (1 : 1 ratio of sulfonate : imidazolium) is achieved at about 10 wt% of silica. However, since not all the sulfonate groups on the silica nanoparticles are accessible to the imidazolium groups on the polymer chains, we expect a higher content of silica nanoparticles to be required for maximizing the electrostatic interactions in the system.

Rheologically the materials transition from liquid-like to solid-like behavior as the concentration of nanosilica-SO_3H increases (Fig. S2†). At low frequencies, the addition of nanoparticles leads to a significant increase in the storage modulus and corresponding complex viscosity (Fig. 2). This well-known behavior is directly related to the development of an extensive 3D network of the silica nanoparticles within the material.[46] Using the Winter–Chambon criterion,[37,38] of tan δ (*i.e.* G''/G') being independent of frequency (Fig. S3†), we find that the materials exhibit gel-like behavior at loadings between 10 and 20 wt% of silica nanoparticles, which also corresponds to the

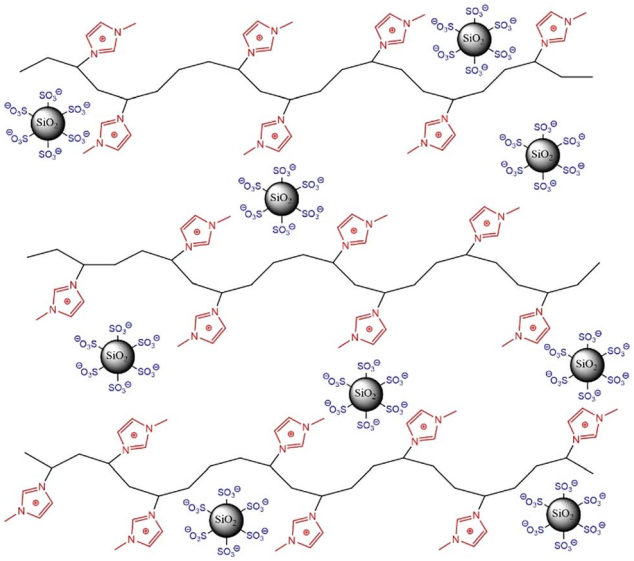

Fig. 1 Ionic nanocomposites synthesized *via* self-assembly of imidazolium-functionalized polyurethanes with sulfonate-modified silica nanoparticles.

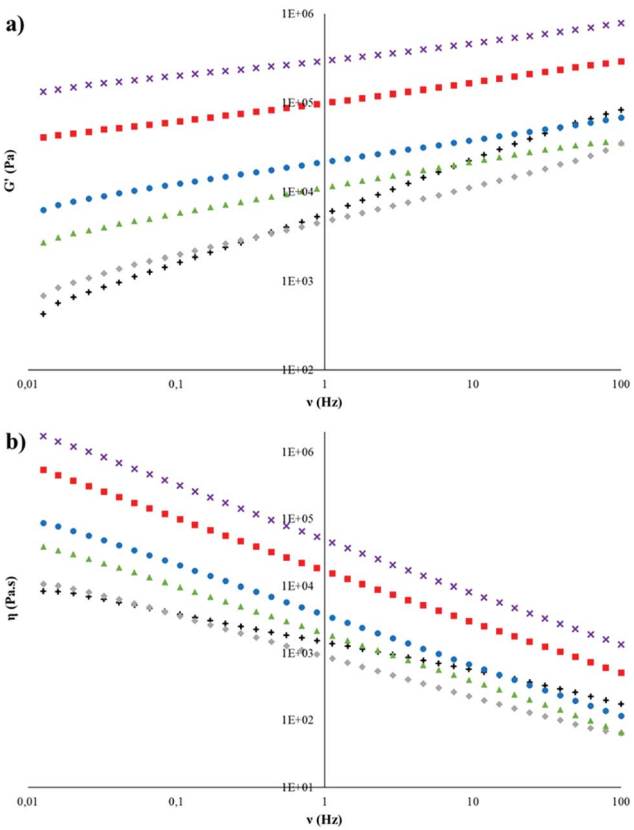

Fig. 2 Storage modulus G' (a) and complex viscosity η (b) as a function of frequency, ν, of neat polymer (black, plus signs) and nanocomposites containing 5 wt% (grey, diamonds), 10 wt% (green, triangles), 20 wt% (blue, circles), 30 wt% (red, squares) and 40 wt% (purple, crosses) of silica nanoparticles.

ratio of imidazolium : sulfonate groups required for charge balance.[47,48]

TEM studies show the nanocomposites to be well dispersed, a typical challenge of conventional, non-ionic based nanocomposites (Fig. S4†). Despite the high silica loadings, the hybrids show good dispersion, which we attribute to the presence of electrostatic interactions in the system. Recall that charge balance requires approximately 20 wt% of silica nanoparticles. At higher silica loadings (>20 wt%), some aggregation is observed reinforcing the critical importance of ionic interactions for achieving good dispersion.

Stiff, tough and stretchy

The presence of ionic interactions endows the hybrids with an unpreceded set of properties. The nanocomposites show significant improvements in modulus, toughness and strain at break compared to the neat polymer (Fig. 3 and Table S1†). This is a remarkable behavior as improvements in modulus in most nanocomposite systems are typically accompanied by a decrease in elongation and toughness. Specifically, the im-PU nanocomposites containing 10 wt% and 20 wt% of silica exhibit *ca.* a 10-fold increase in strain at break (412% and 463% respectively *vs.* 44% for the neat polymer) together with a 30 to 40-fold increase in toughness (10 MJ m^{-3} and 12 MJ m^{-3} *vs.* 0.3 MJ m^{-3}) and a 2.5-fold increase in modulus (30 MPa and 27 MPa *vs.* 12 MPa). The improvements in mechanical properties seem to reach a plateau at about 20 wt%. This range corresponds with the silica to polymer ratio required for charge-balance and before nanoparticle aggregation. It is worth noting that higher silica loadings do not lead to better performance. Recall that higher silica loadings do not lead to more imidazolium–sulfonate interactions, which we believe responsible for the significant properties improvement. Likewise, replacing the nanosilica-SO_3H with its sodium counterpart (–SO_3Na) is not as effective. The electrostatic interactions are screened by the much larger sodium ions when nanosilica-SO_3H is replaced with its sodium form (–SO_3Na) disrupting and decreasing the extent of the interactions in the system. As a result, a drop in the mechanical properties occurs (*e.g.* 177% *vs.* 463% strain at break at 20 wt% for –SO_3Na and –SO_3H, respectively), confirming the critical nature of not only having the ionic motif present but also having the suitable counterion in the ionic system. We attribute the mechanism by which the new nanocomposite systems dissipate strain energy to the dissociation dynamics of the ionic crosslinks[49,50] as well as motion of the nanoparticles under applied stress.[51,52] Since the electrostatic interactions between imidazolium–sulfonate groups are dynamic, the progressive breaking and remaking of the ionic linkages drive the nature of the stress–strain curves at low loading rates.[49,50] Besides, the nanoparticles are mobile enough (facilitated by the relatively low T_m polymer matrix) to create temporary crosslinks between the polymer chains, providing a localized region of enhanced strength, which in turn can retard the growth of cracks and result in large energy dissipation.[51,52] We believe that this mechanism is responsible for simultaneous increases in modulus and extensibility (and toughness) in the ionic nanocomposite systems (comparing, for example, the modulus of 27 MPa and strain to failure of 463% *vs.* 12 MPa and 44% for the 20 wt% and 0 wt% SiO_2–SO_3H systems, respectively).

In addition, the tensile behavior of the nanocomposites dramatically changes with the loading rate (Fig. 4 and Table S2†). As is typical, the strain at break for the neat im-PU decreases as the loading rate increases. In contrast, the nanocomposites not only can sustain much higher levels of strain but also show better performance at high loading rates. For instance, as the loading rate increases from 10 to 1000 mm min^{-1} the strain at break increases from 463 to 558% (the corresponding toughness increases from 12 to 19 MJ m^{-3}). While we cannot unequivocally rationalize the strain rate behavior at present, we hypothesize that it is also the result of the ionic nature of the system. The absence of these electrostatic interactions from the neat im-PU leads to low strain at failure values. Similarly, the presence of only covalent bonds in

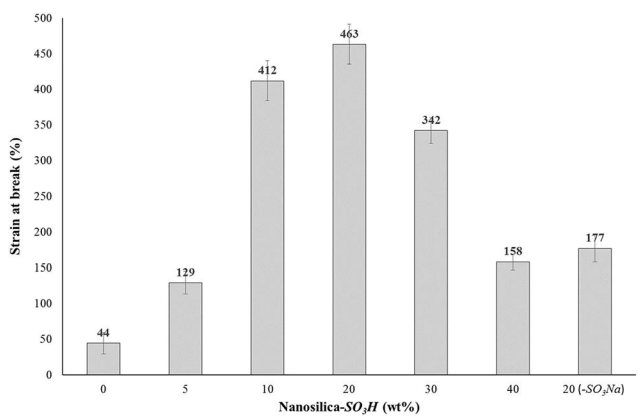

Fig. 3 Strain at break of the neat polymer and nanocomposites with different silica nanoparticle loadings.

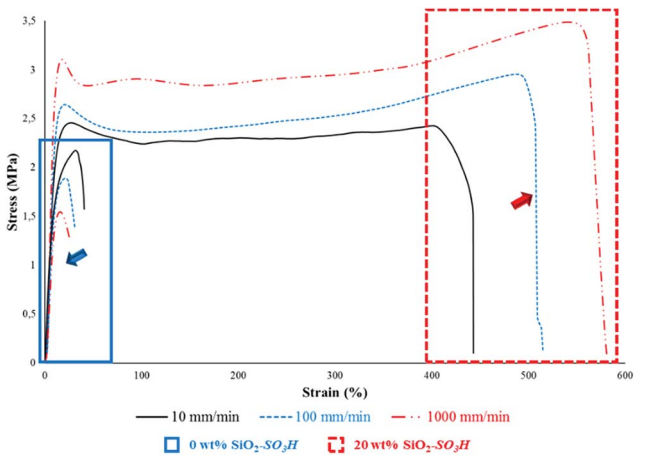

Fig. 4 Typical stress–strain curves of the neat polymer (solid blue square) and the nanocomposite containing 20 wt% of nanosilica (dashed red square) at different strain rates: 10 mm min^{-1} (solid black line), 100 mm min^{-1} (dashed blue line) and 1000 mm min^{-1} (dash-dotted red line).

This journal is © The Royal Society of Chemistry 2017

neat im-PU results in the well-known trend of lower elongation with modest increase in modulus as the deformation rate increases. The ionic interactions act as dynamic crosslinks resulting in an elastic nanocomposite with high modulus and extensibility with the relaxation times of these dynamic crosslinks probably in the range of applied strain rates. Clearly, further studies are necessary to elucidate the exact mechanism so that a more detailed analysis to relate the strain-dependent behavior with the dynamic nature of the system. Although DSC and XRD experiments showed virtually no changes in the polymer crystallinity before and after stress loading (see Fig. S5†) we cannot rule out the possibility, since changes induced by stress might be reversible, when the stress is removed, resulting in the same degree of crystallization.

Shape recovery

Due to the reversible nature of the electrostatic imidazolium–sulfonate interactions, the resulting materials can recover their initial state after experiencing a large deformation (Fig. 5). A typical shape-memory polymer (SMP) possesses a stable network, which is responsible for retaining the permanent shape, and a switching network, which is responsible for fixing and releasing the temporary shape through a suitable transition temperature.[53] Temperature is typically used to trigger shape-memory behavior. Hot programming involves heating above the glass (T_g) or melting (T_m) transition, for amorphous and semi-crystalline polymers, respectively. More recently, cold programming has been used, in which the polymer is deformed below the transition zone.[40] Since the $T_g = -55$ °C and $T_m =$ 40 °C for our system and the nanocomposites are highly deformable at room-temperature (*i.e.* below T_m using cold programming), they were first stretched to a strain of 200% by applying a constant deformation. This deformation leads to a large internal stress stored in a temporary pre-deformed shape. The subsequent release of the residual stress at room-temperature (*i.e.* low-temperature unloading) drives the elastic rebound (with a relaxation occurring within a few seconds, see Fig. 5b) thanks to the entropic relaxation of the polymer chains,[54,55] after which a large percentage of plastic deformation remains. The amount of elastic rebound is supposed to reflect the shape fixity ratio, with a longer holding time leading to larger shape-fixity.[40,56,57] Subsequent heating to 50 °C (*i.e.* above its melting transition T_m) allows the sample to recover its original shape through reversible plasticity (with a relaxation occurring within minutes, see Fig. 5b) – a form of shape memory, where large plastic deformation at room temperature is fully recoverable upon heating.[58] The recoverable strain as compared with the residual visco-plasto-damage strain defines the shape recovery capability of the materials.[40] Table 1 summarizes the shape recovery performance of the nanocomposites as quantified by DMTA. From these measurements, neat im-PU only sustained low and irreversible deformation during the shape-memory process. In contrast, the nanocomposites demonstrated remarkable reversibility even after substantial deformations. For instance, the 20 wt% nanosilica-SO_3H nanocomposite achieved a full shape-recovery (*i.e.* R_r and

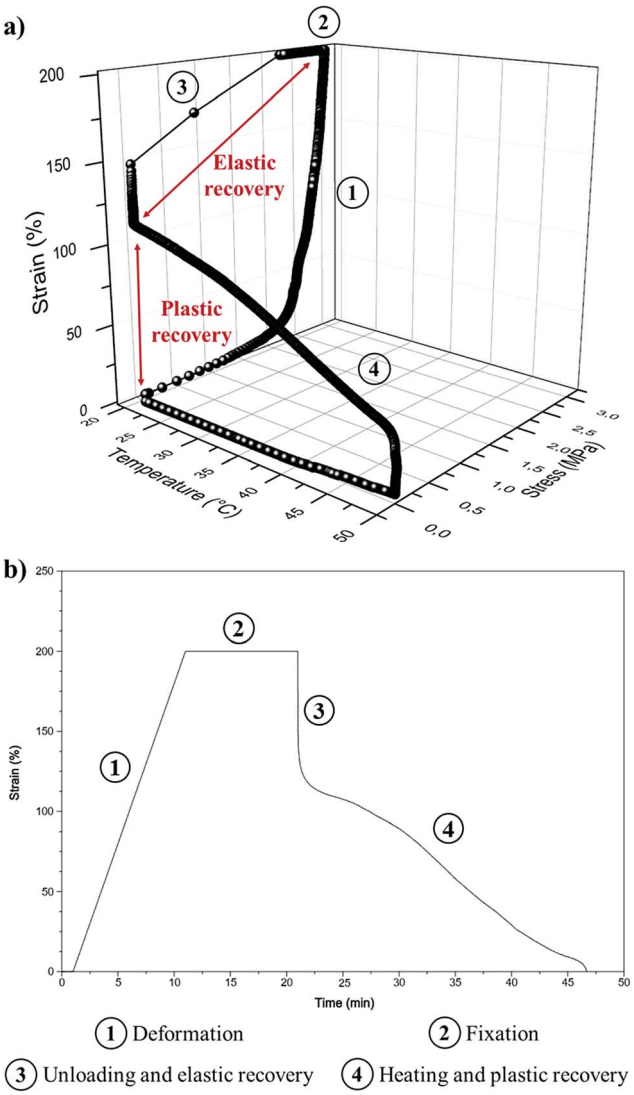

Fig. 5 Cyclic stress-controlled thermomechanical test (DMTA) of the nanocomposite containing 20 wt% of nanosilica showing (a) reversible plasticity/shape-memory and (b) the relaxation time required to achieve complete shape recovery.

C_{tot} of 100%) through both elastic and plastic contributions with $C_{elas} = 45\%$ and $C_{plas} = 55\%$, respectively. As noted earlier, this particular composition corresponds with the silica to

Table 1 Shape recovery performances of nanocomposites with different silica nanoparticle loadings[a]

SiO_2–SO_3H content (wt%)	C_{elas} (%)	C_{plas} (%)	C_{tot} (%)	R_f (%)	R_r (%)
0	*	*	*	*	*
5	*	*	*	*	*
10	34	38	72	66	57
20	45	55	100	55	100
30	43	37	80	57	65
40	*	*	*	*	*

[a] * Not determined – the neat polymer and the nanocomposite based on 5 wt% and 40 wt% silica cannot be stretched to 200% of strain.

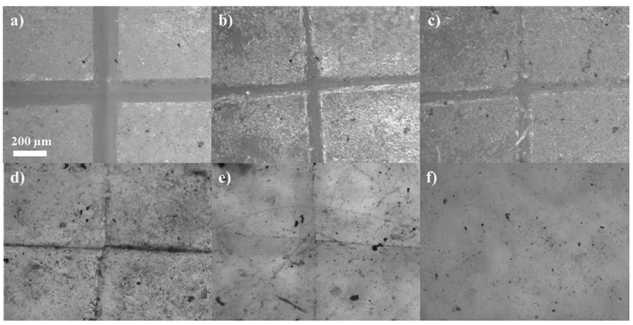

Fig. 6 Scratch recovery behavior of nanocomposites containing 20 wt% of nanosilica immediately after scratching (a) and after being held at 50 °C for 1 h (b), 2 h (c), 3 h (d), 4 h (e) and 5 h (f).

polymer ratio required for charge-balance and before nanoparticle aggregation.

Scratch recovery

In our design, we envisioned that the dynamic and reversible imidazolium–sulfonate bonding should also afford self-healing properties. In this respect, nanocomposites containing 20 wt% of nanosilica-SO_3H showed remarkable self-healing ability (Fig. 6). After scratching the sample with a razor blade (scratch of *ca.* 500 μm depth and 160 μm width) and gently bringing the two cut pieces back into contact, the two faces spontaneously healed upon heating at 50 °C. Longer healing times lead to better self-healing, ensuring a full scratch recovery after *ca.* 4 h. In contrast to our system, most approaches to self-healing materials require systems with enough mobility at the molecular level, which usually impacts their inherent stiffness.[59,60]

Conclusions

Ionic nanocomposites based on imidazolium-functionalized polyurethanes (im-PUs) and surface-modified sulfonated silica nanoparticles (nanosilica-SO_3H) were synthesized and their multi-responsive and adaptable properties were characterized. Rheologically the materials transition from liquid-like to solid-like behavior as the concentration of nanosilica-SO_3H increases, confirming the establishment of an extensive 3D particle network within the system. The presence of ionic interactions endows the materials with good levels of dispersion of the nanoparticles in the polymer despite the high silica loadings. As a result, stiff, tough and highly stretchable nanocomposite materials are obtained. For instance, loading 20 wt% of nanosilica-SO_3H led to well-dispersed hybrids with an 11-fold increase in strain at break, a 40-fold increase in tensile toughness and a 2.5-fold increase in stiffness compared to the neat polymer. Surprisingly, the nanocomposites not only sustain higher levels of strain but also show better response at larger loading rates. Thanks to the dynamic and reversible nature of the ionic imidazolium–sulfonate crosslinks present, the nanocomposites show remarkable reversible plasticity/shape-recovery (*i.e.* they fully recover their initial state even after substantial deformations). Finally, the nanocomposites exhibit self-healing behavior. All in all the ionic nanocomposites lead to a unique property profile that combines simultaneous improvements in stiffness, toughness and extensibility. In addition, the nanocomposites exhibit unique strain-dependent behavior (*i.e.* the deformation increases with increasing strain rate) and return to the normal state after deformation including not only shape-memory but also scratch recovery. We attribute this unique behavior to the presence of ionic interactions, which act as dynamic crosslinks resulting in an elastic nanocomposite with high modulus and extensibility and with relaxation times of these dynamic crosslinks probably in the range of applied strain rates.

Acknowledgements

J. Odent gratefully thanks the Belgian American Educational Foundation (BAEF) for its financial support. J -M. Raquez is a research associate from F.R.S.-FNRS (Belgium). We gratefully acknowledge support from NPRP Grant # 5-1437-1-243 from Qatar National Research Fund. We also acknowledge use of facilities at the Cornell Center for Materials Research (CCMR) supported by the National Science Foundation under Award No. DMR-1120296 and the support of Award No. KUS-C1-018-02 made by King Abdullah University of Science and Technology (KAUST).

Notes and references

1 J.-M. Lehn, *Chem. Soc. Rev.*, 2007, **36**, 151–160.
2 R. J. Wojtecki, M. A. Meador and S. J. Rowan, *Nat. Mater.*, 2011, **10**, 14–27.
3 S. J. Rowan, S. J. Cantrill, G. R. L. Cousins, J. K. M. Sanders and J. F. Stoddart, *Angew. Chem., Int. Ed.*, 2002, **41**, 898–952.
4 P. Cordier, F. Tournilhac, C. Soulie-Ziakovic and L. Leibler, *Nature*, 2008, **451**, 977–980.
5 H. Ying, Y. Zhang and J. Cheng, *Nat. Commun.*, 2014, **5**, 3218.
6 J. Li, J. A. Viveros, M. H. Wrue and M. Anthamatten, *Adv. Mater.*, 2007, **19**, 2851–2855.
7 M. A. C. Stuart, W. T. S. Huck, J. Genzer, M. Muller, C. Ober, M. Stamm, G. B. Sukhorukov, I. Szleifer, V. V. Tsukruk, M. Urban, F. Winnik, S. Zauscher, I. Luzinov and S. Minko, *Nat. Mater.*, 2010, **9**, 101–113.
8 R. Vaia and J. Baur, *Science*, 2008, **319**, 420–421.
9 F. Liu and M. W. Urban, *Prog. Polym. Sci.*, 2010, **35**, 3–23.
10 K. P. Nair, V. Breedveld and M. Weck, *Macromolecules*, 2008, **41**, 3429–3438.
11 Y. Chen and Z. Guan, *Chem. Commun.*, 2014, **50**, 10868–10870.
12 T. Ware, K. Hearon, A. Lonnecker, K. L. Wooley, D. J. Maitland and W. Voit, *Macromolecules*, 2012, **45**, 1062–1069.
13 D. C. Tuncaboylu, M. Sari, W. Oppermann and O. Okay, *Macromolecules*, 2011, **44**, 4997–5005.
14 A. Ustinov, H. Weissman, E. Shirman, I. Pinkas, X. Zuo and B. Rybtchinski, *J. Am. Chem. Soc.*, 2011, **133**, 16201–16211.

 This journal is © The Royal Society of Chemistry 2017

15 E. Obert, M. Bellot, L. Bouteiller, F. Andrioletti, C. Lehen-Ferrenbach and F. Boué, *J. Am. Chem. Soc.*, 2007, **129**, 15601–15605.
16 Q. Wang, Y. Bai, Y. Chen, J. Ju, F. Zheng and T. Wang, *J. Mater. Chem. A*, 2015, **3**, 352–359.
17 S. Burattini, B. W. Greenland, D. H. Merino, W. Weng, J. Seppala, H. M. Colquhoun, W. Hayes, M. E. Mackay, I. W. Hamley and S. J. Rowan, *J. Am. Chem. Soc.*, 2010, **132**, 12051–12058.
18 G. R. Whittell, M. D. Hager, U. S. Schubert and I. Manners, *Nat. Mater.*, 2011, **10**, 176–188.
19 C.-F. Chow, S. Fujii and J.-M. Lehn, *Angew. Chem., Int. Ed.*, 2007, **46**, 5007–5010.
20 T. L. Sun, T. Kurokawa, S. Kuroda, A. B. Ihsan, T. Akasaki, K. Sato, M. A. Haque, T. Nakajima and J. P. Gong, *Nat. Mater.*, 2013, **12**, 932–937.
21 J.-Y. Sun, X. Zhao, W. R. K. Illeperuma, O. Chaudhuri, K. H. Oh, D. J. Mooney, J. J. Vlassak and Z. Suo, *Nature*, 2012, **489**, 133–136.
22 O. Jaudouin, J.-J. Robin, J.-M. Lopez-Cuesta, D. Perrin and C. Imbert, *Polym. Int.*, 2012, **61**, 495–510.
23 N. Hohlbein, M. von Tapavicza, A. Nellesen and A. M. Schmidt, in *Self-Healing Polymers*, Wiley-VCH Verlag GmbH & Co. KGaA, 2013, pp. 315–334, DOI: 10.1002/9783527670185.ch13.
24 M. Capelot, D. Montarnal, F. Tournilhac and L. Leibler, *J. Am. Chem. Soc.*, 2012, **134**, 7664–7667.
25 W. Denissen, M. Droesbeke, R. Nicolaÿ, L. Leibler, J. M. Winne and F. E. Du Prez, *Nat. Commun.*, 2017, **8**, 14857.
26 M. Capelot, M. M. Unterlass, F. Tournilhac and L. Leibler, *ACS Macro Lett.*, 2012, **1**, 789–792.
27 L. Zhang, N. R. Brostowitz, K. A. Cavicchi and R. A. Weiss, *Macromol. React. Eng.*, 2014, **8**, 81–99.
28 C. L. Lewis and E. M. Dell, *J. Polym. Sci., Part B: Polym. Phys.*, 2016, **54**, 1340–1364.
29 K. A. Cavicchi, M. Pantoja and M. Cakmak, *J. Polym. Sci., Part B: Polym. Phys.*, 2016, **54**, 1389–1396.
30 L. Lu and G. Li, *ACS Appl. Mater. Interfaces*, 2016, **8**, 14812–14823.
31 R. Dolog and R. A. Weiss, *Macromolecules*, 2013, **46**, 7845–7852.
32 R. J. Varley and S. van der Zwaag, *Acta Mater.*, 2008, **56**, 5737–5750.
33 A. B. Bourlinos, R. Herrera, N. Chalkias, D. D. Jiang, Q. Zhang, L. A. Archer and E. P. Giannelis, *Adv. Mater.*, 2005, **17**, 234–237.
34 R. Rodriguez, R. Herrera, L. A. Archer and E. P. Giannelis, *Adv. Mater.*, 2008, **20**, 4353–4358.
35 R. Rodriguez, R. Herrera, A. B. Bourlinos, R. Li, A. Amassian, L. A. Archer and E. P. Giannelis, *Appl. Organomet. Chem.*, 2010, **24**, 581–589.
36 N. J. Fernandes, J. Akbarzadeh, H. Peterlik and E. P. Giannelis, *ACS Nano*, 2013, **7**, 1265–1271.
37 N. J. Fernandes, T. J. Wallin, R. A. Vaia, H. Koerner and E. P. Giannelis, *Chem. Mater.*, 2014, **26**, 84–96.
38 M. L. Jespersen, P. A. Mirau, E. v. Meerwall, R. A. Vaia, R. Rodriguez and E. P. Giannelis, *ACS Nano*, 2010, **4**, 3735–3742.
39 J. Odent, J.-M. Raquez, C. Samuel, S. Barrau, A. Enotiadis, P. Dubois and E. P. Giannelis, *Macromolecules*, 2017, **50**, 2896–2905.
40 G. Li and A. Wang, *J. Polym. Sci., Part B: Polym. Phys.*, 2016, **54**, 1319–1339.
41 T. Peppel and M. Köckerling, *Z. Anorg. Allg. Chem.*, 2011, **637**, 870–874.
42 J. Hu, T. Kurokawa, T. Nakajima, T. L. Sun, T. Suekama, Z. L. Wu, S. M. Liang and J. P. Gong, *Macromolecules*, 2012, **45**, 9445–9451.
43 T. C. Suekama, J. Hu, T. Kurokawa, J. P. Gong and S. H. Gehrke, *ACS Macro Lett.*, 2013, **2**, 137–140.
44 T. Nakajima, Y. Fukuda, T. Kurokawa, T. Sakai, U.-i. Chung and J. P. Gong, *ACS Macro Lett.*, 2013, **2**, 518–521.
45 J. Hu, T. Kurokawa, T. Nakajima, Z. L. Wu, S. M. Liang and J. P. Gong, *Macromolecules*, 2014, **47**, 3587–3594.
46 T. Domenech, R. Zouari, B. Vergnes and E. Peuvrel-Disdier, *Macromolecules*, 2014, **47**, 3417–3427.
47 H. H. Winter and F. Chambon, *J. Rheol.*, 1986, **30**, 367–382.
48 F. Chambon and H. H. Winter, *J. Rheol.*, 1987, **31**, 683–697.
49 K. Mayumi, A. Marcellan, G. Ducouret, C. Creton and T. Narita, *ACS Macro Lett.*, 2013, **2**, 1065–1068.
50 R. Long, K. Mayumi, C. Creton, T. Narita and C.-Y. Hui, *Macromolecules*, 2014, **47**, 7243–7250.
51 D. Gersappe, *Phys. Rev. Lett.*, 2002, **89**, 058301.
52 D. Shah, P. Maiti, D. D. Jiang, C. A. Batt and E. P. Giannelis, *Adv. Mater.*, 2005, **17**, 525–528.
53 M. D. Hager, S. Bode, C. Weber and U. S. Schubert, *Prog. Polym. Sci.*, 2015, **49–50**, 3–33.
54 J. Leng, X. Lan, Y. Liu and S. Du, *Prog. Mater. Sci.*, 2011, **56**, 1077–1135.
55 F. Pilate, R. Mincheva, J. De Winter, P. Gerbaux, L. Wu, R. Todd, J.-M. Raquez and P. Dubois, *Chem. Mater.*, 2014, **26**, 5860–5867.
56 M. Behl and A. Lendlein, *Mater. Today*, 2007, **10**, 20–28.
57 T. Xu and G. Li, *Polymer*, 2011, **52**, 4571–4580.
58 E. D. Rodriguez, X. Luo and P. T. Mather, *ACS Appl. Mater. Interfaces*, 2011, **3**, 152–161.
59 N. R. Sottos and J. S. Moore, *Nature*, 2011, **472**, 299–300.
60 Y. Chen, A. M. Kushner, G. A. Williams and Z. Guan, *Nat. Chem.*, 2012, **4**, 467–472.